Korean J. Chem. Eng., 32(7), 1414-1421 (2015)
DOI: 10.1007/s11814-014-0346-2

pISSN: 0256-1115
eISSN: 1975-7220

Computational fluid dynamics modeling and analysis of Pd-based membrane module for CO_2 capture from H_2/CO_2 binary gas mixture

Dong-Yoon Shin*, Kyung-Ran Hwang, Jong-Soo Park***, and Myung-June Park*,****,†**

*Department of Energy Systems Research, Ajou University, Suwon 443-749, Korea
**Clean Fuel Department, Korea Institute of Energy Research, Daejeon 305-343, Korea
***Energy Materials Center, Korea Institute of Energy Research, Daejeon 305-343, Korea
****Department of Chemical Engineering, Ajou University, Suwon 443-749, Korea
(*Received 11 September 2014 • accepted 23 November 2014*)

Abstract−A Pd-based membrane module for the capture of CO_2 from a H_2/CO_2 binary gas mixture was considered, and computational fluid dynamics modeling was used to predict the module performance. Detailed models of momentum and mass balances, including local flux as a function of local linear velocity, satisfactorily described CO_2 fraction in a retentate tube when compared to the experimental data under various feed flow rates. By using the model, several cases having different geometries, including the location and diameter of feed tube and the number and location of the feed and retentate tubes, were considered. Among tested geometries, the case of two feed tubes with each offset by an angle, θ, of 45° from the center line, and a feed tube diameter of 2.45 mm showed the increase of the feed flow rate up to 11.80% compared to the reference case while a CO_2 fraction of 90% in the retentate, which was the criterion for effective CO_2 capture in the present study, was guaranteed. This would result in a plausible reduction in capital expenditures for the CO_2 capture process.

Keywords: Pd-based Membrane, CO_2 Capture, Computational Fluid Dynamics Model, H_2 Flux, Module Structure

INTRODUCTION

Concerns about the emission of greenhouse gases into the atmosphere as a result of the use of fossil fuels as a primary energy source have motivated the development of novel methods to capture CO_2 before it could enter the atmosphere [1,2]. CO_2 capture is classified into three categories: post-combustion, pre-combustion, and oxy-fuel combustion. In pre-combustion, fuel is converted to synthesis gas (syngas, mainly CO and H_2) by gasification or reforming, which is followed by the water-gas shift reaction to arrive at a gas rich in H_2 and poor in CO; then, CO_2 is separated from the H_2 mixture. In this method, H_2 selective membranes have frequently been studied in membrane reactors for the water-gas shift and steam reforming reactions [2-5]. Pd-based materials are commonly accepted to be the most suitable in these processes because of their high hydrogen permeability and chemical compatibility with hydrocarbon-containing gas streams [6]. In contrast, pressure swing adsorption (PSA) and cryogenic distillation processes, which are commercially available, are highly energy intensive [7,8].

The design of a membrane module is of great importance in the development of highly efficient membrane processes [9], and the modeling of hydrogen permeation through Pd-alloy membranes is critical to optimizing the operating conditions [10,11]. In addition, the resistances to heat and mass transfer become increasingly significant with high fluxes, and these features necessitate a fundamental understanding of the prevailing heat and mass transfer phenomena [12]. Using computational fluid dynamics (CFD), Takaba and Nakao [9] modeled actual fluid dynamics in complex geometries, and considered the concentration polarization effect as a function of the feed rate, selectivity, operating pressure, mass transfer coefficient, and module geometry. Caravella et al.'s model [10] included the external mass transfer in the multicomponent gaseous phases on both sides of the membrane; the diffusion in the Pd-alloy layer was modeled by the irreversible thermodynamics theory, taking the hydrogen chemical potential as the driving force of the diffusion in the metallic bulk. Coroneo et al. [13] calculated the H_2 permeation with respect to the local determination of the mass transfer resistances offered by both the gas phase and the membrane, to enhance the performance of the model. Miguel et al. [6] proposed a rearrangement of the Sieverts-Langmuir (SL) equation to account for the inhibition effect on the membrane permeance toward H_2 because of the presence of CO or CO_2, finding that carbon monoxide had a much stronger inhibition effect on hydrogen permeation than carbon dioxide. Boon et al. [12] showed that accurate scale-up and performance predictions for membranes strongly depended on an adequate representation of the prevailing resistances to mass transfer, and the requirement for a two-dimensional model was corroborated. Chen et al. [14] developed a two-dimensional numerical method to determine the feasibility of Sieverts' law and to simulate the phenomenon of concentration polarization for hydrogen permeation in a Pd-based membrane tube. They extended their research, finding that baffles equipped in the shell were conducive to disturbing the H_2 concentration boundary layer and reducing the concentration polarization at the retentate, thereby intensify-

†To whom correspondence should be addressed.
E-mail: mjpark@ajou.ac.kr

ing H_2 permeation [7].

Most of the reported results focused on the effect of membrane size on the flux, but few works have applied the detailed modeling approach on the basis of CFD model to suggest an effective geometry for increasing separation capacity. We have developed a detailed model that describes the CO_2 capture module using a Pd-based composite membrane. Further, after its validity was proven by comparison with experimental data, the model was used to evaluate how different module configurations, such as the number and the location of tubes, affected the separation performance. Since the increase of the module capacity was assumed to be based on the numbering up of each separation membrane, the effect of the membrane size was not considered in the present study. Meanwhile, the increase of the efficiency of one membrane reduces the number of membranes in the module for the fixed capacity, resulting in the decrease of the capital cost, and thus, the module based on the CFD modeling was analyzed in the present study.

EXPERIMENTAL

1. Pd-Au Membrane Preparation and Configuration of Membrane Module

A plate-type Pd-Au membrane (5.0 mm in diameter and 1.5 mm thick) was prepared over a porous metal support by sputtering and sintering procedures, as previously described [3,4]. The porous nickel metal support was simply prepared by uniaxial pressing and sintering processes, and it was polished to reduce its surface roughness using a 0.9 μm alumina slurry. Pd (4 μm) and Au (50 nm) layers were consecutively deposited over the pre-polished support. After the Pd-Au deposition, the plate was sintered at 700 °C for 2 h to increase the density of the Pd-Au layer. More detailed information may be found elsewhere [3,4].

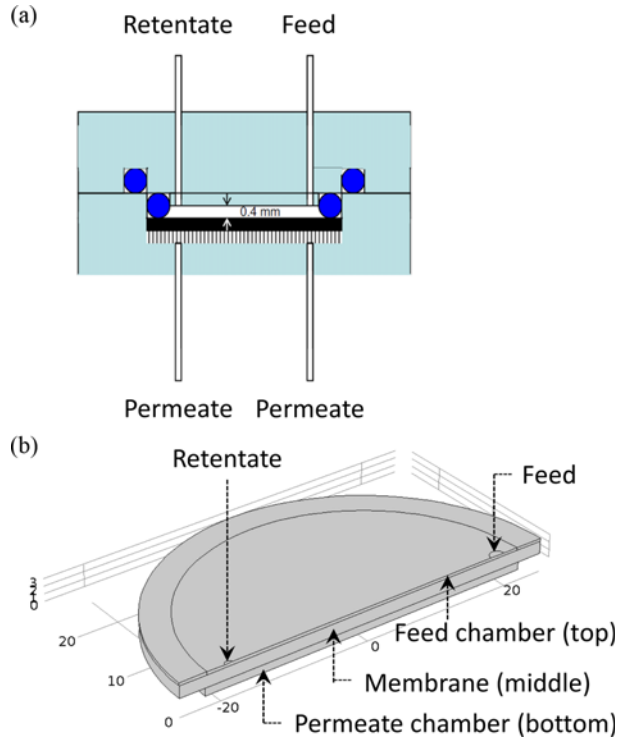

Fig. 1. (a) Schematic diagram of the CO_2 capture module using Pd-based membrane and (b) the structure realized in the COMSOL Multiphysics (COMSOL Inc.) calculations. The unit used in the Fig. 1(b) is mm.

A schematic diagram of the plate-type membrane module is shown in Fig. 1(a). It consisted of cover and bottom flanges, metal O-rings, the membrane, and four holes for the inflow and outflow of gases [2]. The components were tightened with bolts and nuts through the eight holes on the edges of the flanges. Two differently sized metal O-rings were used to seal the module. On the cover plate in the membrane modules, two holes were prepared for the feed and retentate, while two holes were also prepared on the bottom plate for the collection of hydrogen which permeated through the membrane. The membrane was mounted between the two plates; the effective area of the membrane mounted in the module was 14.8 cm^2.

2. Hydrogen Separation Tests in a Membrane Module

Using a gas mixture ($H_2 : CO_2$=6 : 4 on a dry volume basis) that compositionally modeled that by coal gasification followed by the water-gas shift reaction and H_2O removal, hydrogen separation tests (CO_2 extraction tests) were carried out in the modules at 673 K. The trans-membrane pressure difference (ΔP) was 2 MPa, and the permeate side was kept at atmospheric pressure. The total flow rate of the mixture, metered by a digital flow meter (ADM 2000, Agilent Technologies), was varied from 1,400 to 2,400 mL/min. The temperature was controlled with a K-type thermocouple at the surface of the membrane, and the pressure was regulated by a pressure controller (Alicat Scientific) in the stream line of the retentate side. The CO_2 concentration in the retentate side was analyzed by gas chromatography (GC6890, Agilent) using a flame ionization detector. Before the separation test, the membrane modules were heated to 623 K in an Ar and He environment to prevent the occurrence of micro-cracks in the membrane; the inert atmosphere was then displaced by the gas mixture.

RESULTS AND DISCUSSION

1. Mathematical Modeling

COMSOL Multiphysics (COMSOL Inc.), a CFD program, was used for mathematical modeling, wherein detailed levels of mass and momentum balance equations were taken into account. The

Table 1. Specifications of the membrane module and operating conditions in the present study

	Value
Effective membrane area [cm^2]	14.8
Membrane diameter* [mm]	43.4
Retentate tube diameter [mm]	1.0
Feed chamber height [mm]	0.4
Feed tube diameter [mm]	2.0
Flow rate [mL/min]	1400-2400
The trans-membrane pressure difference (ΔP) [MPa]	2.0
Temperature [K]	673

*Calculated from the area of effective membrane

schematic diagram of the experimental module considered in the COMSOL Multiphysics calculations is provided in Fig. 1(b), and information on the module specifications is listed in Table 1. Because of its symmetry, half of the module was considered in the simulation to reduce the computational load.

The COMSOL Multiphysics package includes several computational modules for mass, momentum, and energy balances; the "Free & Porous Media Flow" and "Transport of Concentrated Species" modules were used for the momentum and mass balance computations, respectively, in the present study. The corresponding equations for each module are as follows:

Momentum balance equation:

$$\rho(\mathbf{u}\cdot\nabla)\mathbf{u}=\nabla\cdot\left[-p\mathbf{I}+\mu(\nabla\mathbf{u}+(\nabla\mathbf{u})^{T})-\frac{2}{3}\mu(\mathbf{u}\cdot\nabla)\mathbf{I}\right]+\mathbf{F} \quad (1)$$

Mass balance equation:

$$\nabla\cdot\mathbf{j}_i+\rho(\mathbf{u}\cdot\nabla)\omega_i=R_i \quad (2)$$

where

$$\mathbf{j}_i=-\left(\rho D_i^m\nabla\omega_i+\rho\omega_i D_i^m\frac{\nabla M_m}{M_m}+D_i^T\frac{\nabla T}{T}\right)$$

where the volume force vector (**F**) was assumed to be zero for simplicity, and the reaction rate (R_i) was specified to be zero due to non-existence of the reaction. The other symbols are referred to the Nomenclature section. In addition, the continuity equation was combined with the momentum equation to solve two unknowns; pressure and velocity. Also note that since the mass balance equation is applied to the chamber, porous flow was not considered in the Free & Porous Media Flow module. For numerical analysis, Galerkin's method [15] was applied, and 28,959,231 free tetrahedral grids were defined by specifying the mesh level at "extremely fine". Since the area of the feed and retentate tubes is much smaller than the membrane surface, the highest level was used for enough number of grids in the tubes. Convergence criterion was specified in such a way that the weighted Euclidean norm [16] of the estimated error of the current approximation to the true solution vector (*cf.* the balance Eqs. (1) and (2)) is lower than 1×10^{-3} (default value).

Fluid density in the chamber was expressed, on the basis of the ideal equation of state, as follows:

$$\rho=\frac{P}{RT}(M_{CO_2}x_{CO_2}+M_{H_2}x_{H_2}) \quad (3)$$

Here, P, T, M_i, and x_i represent the pressure, temperature, molar mass, and composition of species i, respectively, and R denotes the gas constant. Because the pressure and temperature in the feed chamber were maintained at 2.1 MPa and 673 K, respectively, the density was determined as a function of local composition. The diffusion coefficient in the mass balance equation was calculated using a binary diffusion coefficient as follows [17]:

$$D_{CO_2\text{-}H_2}=\frac{10^{-3}T^{1.75}[(1/M_{CO_2})+(1/M_{H_2})]^{1/2}}{P[(\sum v)_{CO_2}^{1/3}+(\sum v)_{H_2}^{1/3}]^2} \quad (4)$$

The symbol v represents the atomic diffusion volumes, and the values of $\sum v$ for CO_2 and H_2 are 26.9 and 6.12, respectively [18]. Owing to the isothermal and isobaric conditions, as well as the assumption of a weak function of the composition, the dynamic viscosity was calculated as 2.5605×10^{-5} Pa·s on the basis of the feed composition ($H_2:CO_2=60:40$), and this value was used for the entire simulation study. The feed composition was based on the mixture gas from the coal gasification followed by the water gas shift reaction and H_2O removal.

The H_2 flux (j_{H_2}) was calculated at the boundary between the feed chamber and the membrane, applying the most widely used general expression [14,19]:

$$j_{H_2}=\frac{\dot{m}_{H_2}}{A}=Q(P_r^n-P_p^n)=\frac{Q'}{l}(P_r^n-P_p^n) \quad (5)$$

where the symbols $\dot{m}_{H_2}$, A, and *l* represent the molar flow rate of H_2, surface area, and thickness of the membrane, respectively. Q and Q′ denote the permeance and permeability, respectively. When n=0.5, the equation is called Sieverts' law; however, n mostly ranges between 0.5 and 1.0 because of surface poisoning, grain boundar-

Table 2. Properties of various Pd-based membranes [3,19]

Membrane	*l* [μm]	T [K]	n [-]	Q [mol/(m²·s·Pa^n)]	Reference
Pd/PSS	11.7	623	0.5	2.5×10^{-6}	[20]
Pd/α-Al_2O_3	10.3	850	0.65	3.7×10^{-6}	[21]
Pd/-	20	673	0.5	6.46×10^{-4}	[22]
Pd/PSS	20	593-773	1.0	-	[23]
Pd/PSS	20	623	0.5	2.61×10^{-4}	[24]
$Pd_{46}Cu_{54}$/ZrO_2-PSS	10	593-753	1.0	-	[25]
Pd-Cu/α-Al_2O_3	11	723	1.0	2.32×10^{-6}	[26]
Pd-Ag/Al_2O_3	10	-	1.0	1.0×10^{-6}	[27]
Pd-Ag/α-Al_2O_3	11	823	1.0	1.29×10^{-6}	[28]
Pd-Ag/Al_2O_3	12	773	0.5	1.5×10^{-3}	[29]
Pd/ZrO_2-PSS	10	773	0.5	8.3×10^{-7}	[30]
Pd/CeO_2-PSS	13	823	0.5	1.4×10^{-7}	[31]
Pd/γ-Al_2O_3-α-Al_2O_3	15	673	0.61	8.7×10^{-7}	[32]
Pd/α-Fe_2O_3-PSS	16	673	0.5	8.8×10^{-5}	[33]
Pd/Al_2O_3/PSS	4.4	773	0.5	2.94×10^{-3}	[34]

Table 3. Errors and standard deviations between experimental and simulation results

Flow rate [mL/min]	CO_2 fraction [%]		Absolute relative residual [%]
	Experiment	Simulation	
1400	92.1	92.30	0.22
1600	88	90.01	2.29
1900	85.7	85.70	0.00
2400	80	77.93	2.59
MARR†			1.27
Standard deviation			1.37

†Mean of absolute relative residuals (MARR) [%]

$$=100\times\left(\sum_i |y_{i,exp}-y_{i,cal}|/y_{i,exp}\right)/N_{exp}$$

ies, defects, or microcracks in the metal. Some reported values for n are listed in Table 2.

In the present study, the value of n was specified as 1, and experiments were conducted under the conditions ΔP=2 MPa and T=673 K with variable flow rates, as shown in Table 3, to determine the value of the permeance. The permeance is a characteristic of the membrane and should be independent form the operating conditions, while CO_2 fraction in the retentate was observed to be dependent on the feed flow rate (ΔP and T were fixed). This feature indicates that there exist some effects that influence the membrane performance, but a detailed mechanism could not be suggested. Instead, because the linear velocity in the chamber as well as feed flow rates changed, a correlation between the permeance and the linear velocity was introduced as a correction factor in the present study, as follows:

$$Q=Q_{sf}\left(\frac{u}{u_{sf}}\right)^{\beta} \quad (6)$$

Here, u denotes the linear velocity in the chamber. The subscript "sf" refers to the scaling factor, corresponding to the values at a flow rate of 1,400 mL/min in the present study.

To determine the approximate value of β, it was assumed that

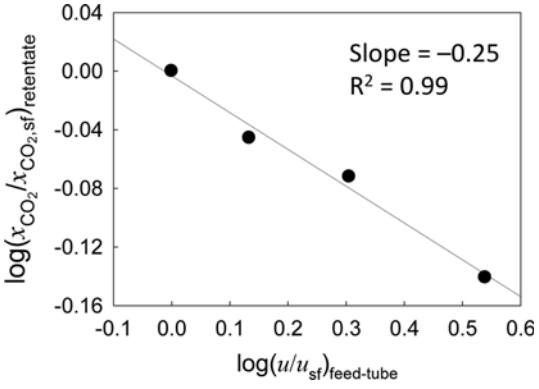

Fig. 2. Plot between the scaled CO_2 fraction in the retentate and the scaled linear velocity of a gas mixture in the feed tube, where the scaling factors were the values obtained at a feed flow rate of 1,400 mL/min.

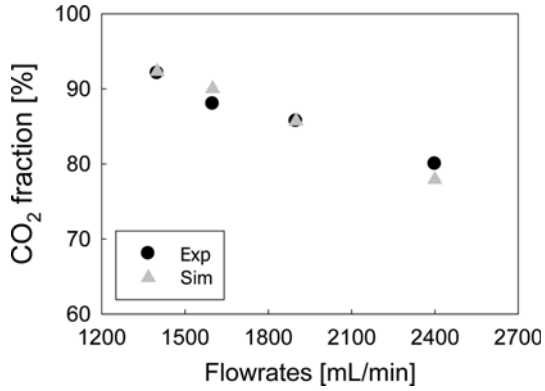

Fig. 3. Comparison of a CO_2 fraction in the retentate between the experimental data and the simulated results.

the CO_2 fraction in the retentate represented the averaged permeance in the chamber, and the ratio of the linear velocities (u/u_{sf}) in the chamber was close to the ratio in the feed tube. Fig. 2 shows the log plot of the experimental data between the scaled CO_2 fraction in the retentate and the linear velocity in the feed tube; the linear regression showed a gradient of −0.251. Therefore, the value of β was assumed to be −0.25.

The value of Q_{sf}, determined by fitting experimental data, was 8.757×10^{-7} mol/(m²·s·Pa). Fig. 3 shows that the simulated results with the permeance as a function of the local linear velocity were in good agreement with the CO_2 fraction in the retentate between the experimental data. As provided in Table 3, the value of the mean of the absolute relative residuals (MARR) was 1.27%.

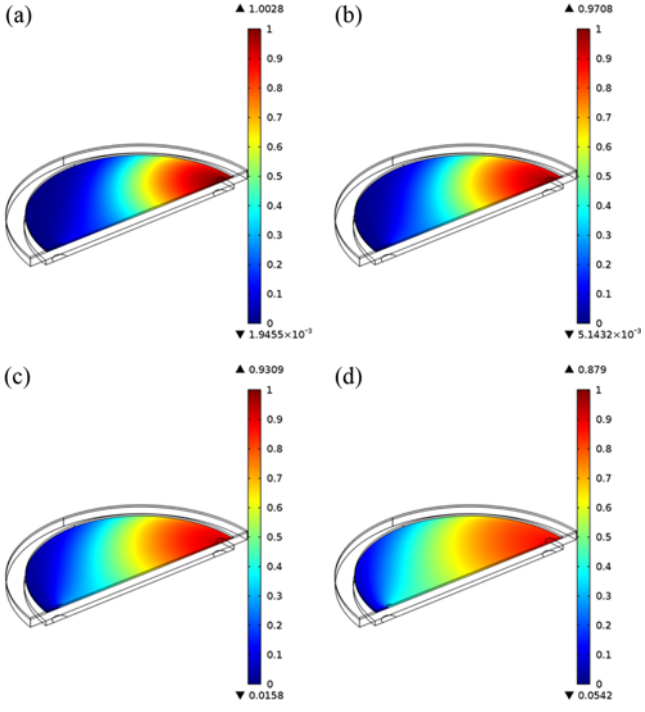

Fig. 4. Calculated values of H_2 flux on the surface of the membrane at flow rates of (a) 1,400, (b) 1,600, (c) 1,900, and (d) 2,400 mL/min.

Fig. 4 shows the H_2 flux at the boundary between the feed chamber and the membrane, where the scales of the color bars were fixed in the same range for the purpose of fair comparison between the cases with different flow rates. At a low flow rate, the maximum value of the flux, provided at the top of the color bar (*e.g.*, maximum H_2 flux=1.0028 mol/(m^2·s) at 1,400 mL/min in Fig. 4(a)), was slightly higher than the high flow rate (*e.g.*, maximum H_2 flux= 0.8790 mol/(m^2·s) at 2,400 mL/min in Fig. 4(d)). Meanwhile, the area with high H_2 flux (the red area) increased with the increasing flow rate, indicating that an increased total amount of H_2 permeated across the membrane owing to the improved utilization of the membrane. However, the degree of increase for the case of high flow rate was not as high, as most of H_2 in the feed could permeate through the membrane and result in a decrease in the CO_2 fraction in the retentate (Fig. 2). Although a binary mixture was considered in the present study, the model can be easily extended to multicomponent feed case since the permeation of hydrogen in the membrane is dependent on the partial pressure of hydrogen.

2. Effects of Membrane Module Structure

As shown in Fig. 4, the greatest utilization of the membrane takes place close to the feed tube, and thus, the location of the feed tube was changed to observe the effects on separation performance. Simulations were conducted for the five different locations indicated in Fig. 5, and the corresponding CO_2 fractions in the retentate are shown in Fig. 6, in which the point with the red star represents the reference conditions (see the caption of Fig. 6 for detailed conditions). Fig. 7 shows that, for locations close to the center, H_2 flux was observed around the center and no flux region (blue color) was large. Therefore, total amount of H_2 was the largest (the highest CO_2 fraction in the retentate) when the feed tube was located close to the side. This may be attributable to the shorter distance between the feed and retentate tubes when the feed tube is located closer to the center, resulting in a decrease in the residence time. Similar behavior has also been reported in the literature [14]. In addition, the location of the feed tube at the center might lead to a problem in maintaining the shape of the chamber, especially when

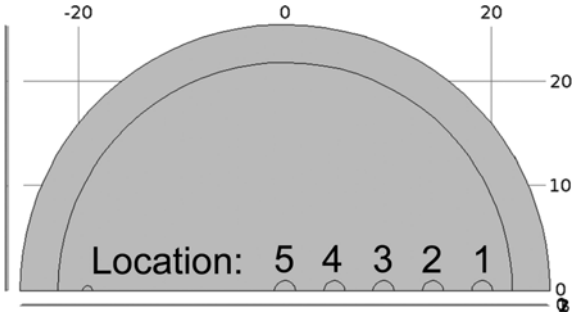

Fig. 5. Scheme for the location of feed tube. Location 5 corresponds to the center, and the distance between the center and Location 1 is 18.875 mm. Locations 2-4 are uniformly distributed between Locations 1 and 5.

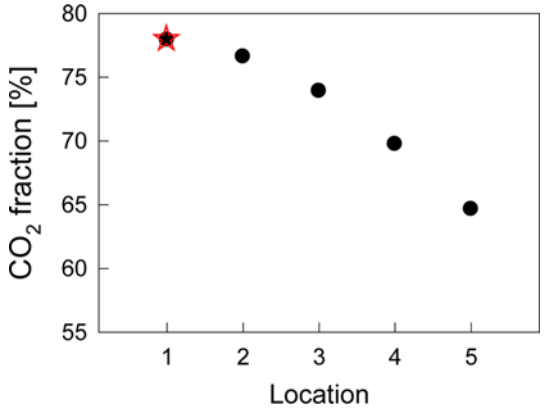

Fig. 6. Effects of different feed tube locations on the CO_2 fraction in the retentate. The red star corresponds to the reference conditions (Location 1, feed tube I.D.=2 mm, the numbers of both feed and retentate tubes=1, flow rate=2,400 mL/min, T=673 K, ΔP=2 MPa).

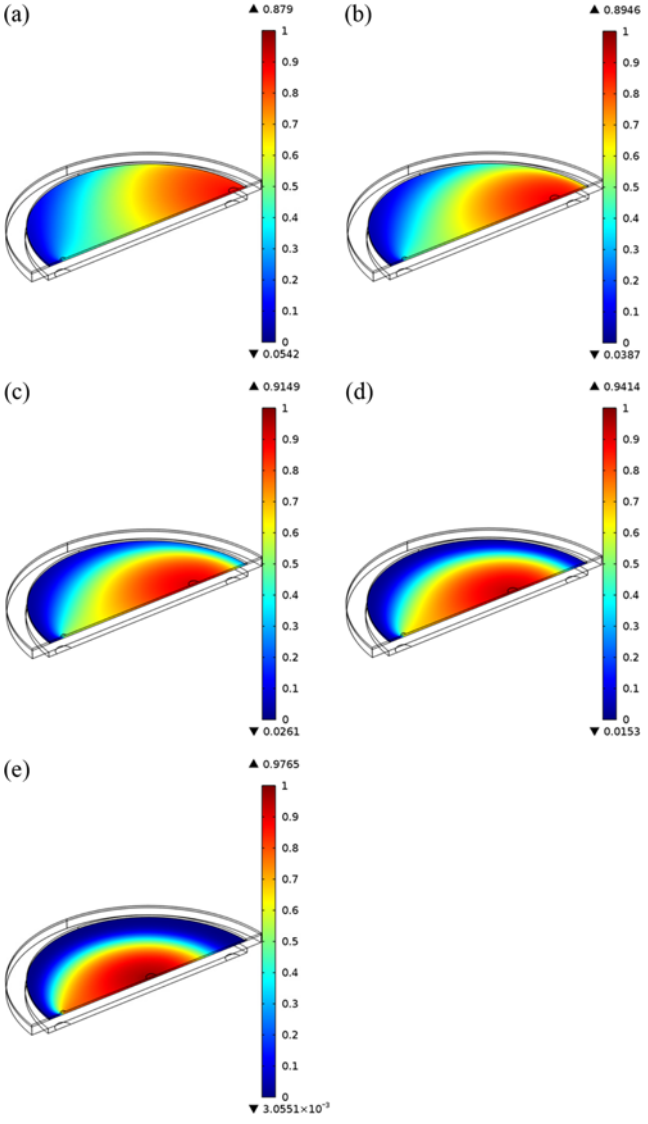

Fig. 7. Calculated values of the H_2 flux on the surface of the membrane under the reference conditions, except for the location of the feed tube at (a) Location 1, (b) Location 2, (c) Location 3, (d) Location 4, and (e) Location 5.

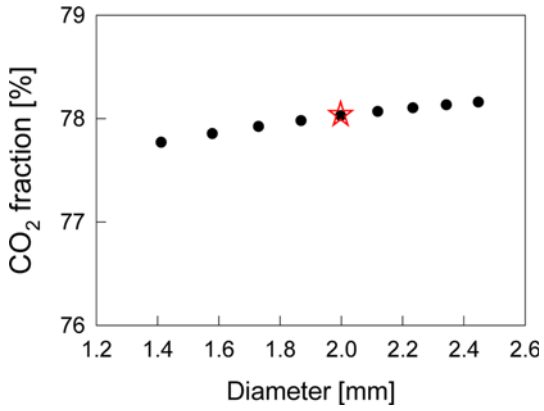

Fig. 8. Effects of the diameter of the feed tube on the CO_2 fraction in the retentate. The red star corresponds to the reference conditions (*cf.* Fig. 6 caption).

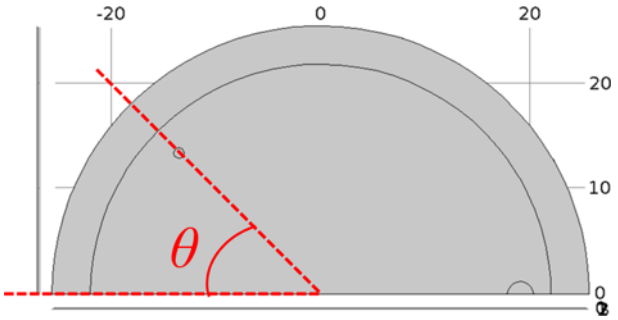

Fig. 9. Definition of θ in the case of two tubes.

the membranes are stacked up for the increase of the module capacity. Therefore, based on the low performance and problem with manufacturing, the location of the feed tube at the center was ruled out.

Another factor in the module configuration is the diameter of the feed tube; its effects are presented in Fig. 8. Because the total flow rate was fixed at 2,400 mL/min for all the conditions, the increase in the feed tube diameter resulted in a decrease in the linear velocity, leading to an increased CO_2 fraction in the retentate. However, the effect of the tube diameter may be negligible, considering that the degree of the change was very small (a relative increase in the fraction by *ca.* 0.64% with a doubling of the tube diameter).

Simulations were carried out by varying the angle between a tube and the center line (θ, Fig. 9) for the case of two tubes, and the results are provided in Fig. 10. The total feed flow rate was fixed and equivalent to the reference conditions, even in the case in which the number of feed tubes was two. When the number of feed and retentate tubes was 2, the values of the maximum CO_2 fraction in the retentate were determined at 45° and 30°, respectively; however, increasing the number of feed tubes was observed to make the maximum CO_2 fraction slightly higher than increase in the number of retentate tubes did. In the case of two feed tubes (Fig. 11), increase in θ from 0° to 45° led to a decrease in the blue region; thus, the utilization of the membrane was increased. However, a further increase in θ prevented the stream from flowing along the center line, re-

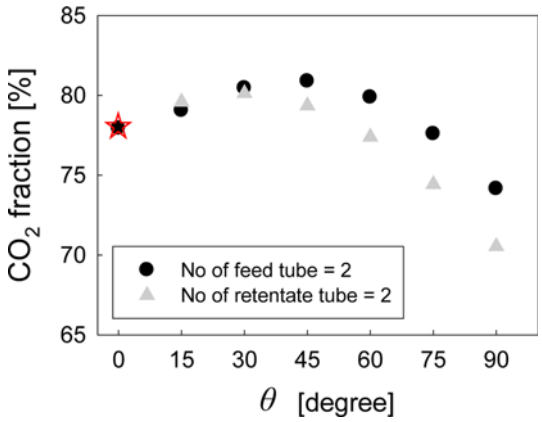

Fig. 10. Effects of the angle between a tube and the center line (θ) on the CO_2 fraction in the retentate when the number of tubes is increased. The red star corresponds to the reference conditions (*cf.* Fig. 6 caption).

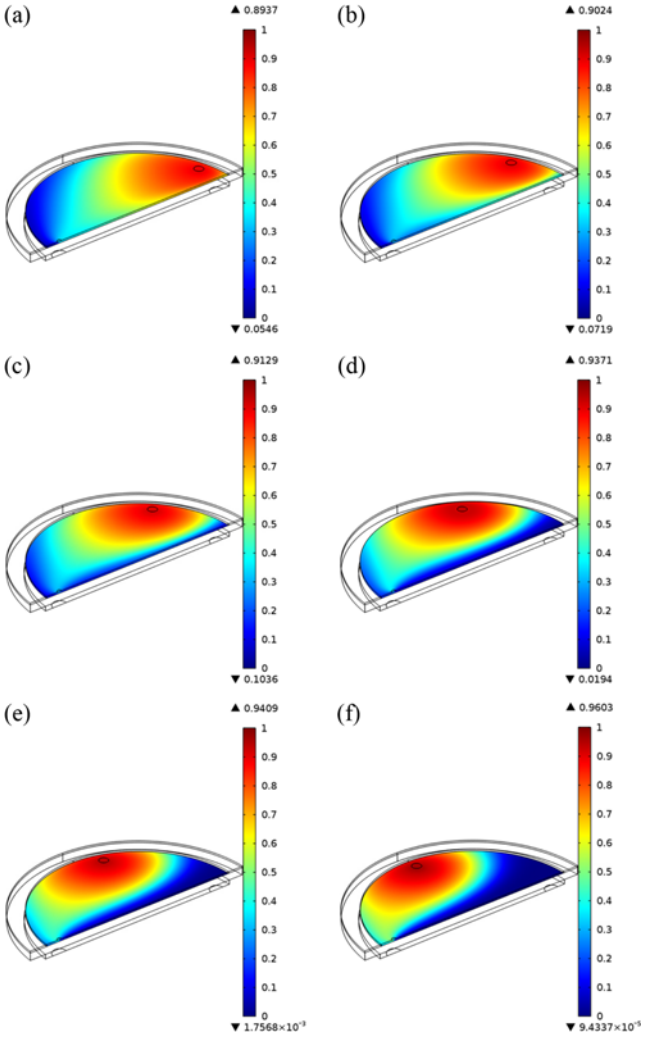

Fig. 11. Calculated values of the H_2 flux on the surface of the membrane when the number of the feed tubes is two and θ is (a) 15°, (b) 30°, (c) 45°, (d) 60°, (e) 75°, and (f) 90°. Due to the symmetry, one feed tube and half of the retentate tube in the center line are shown in the figure.

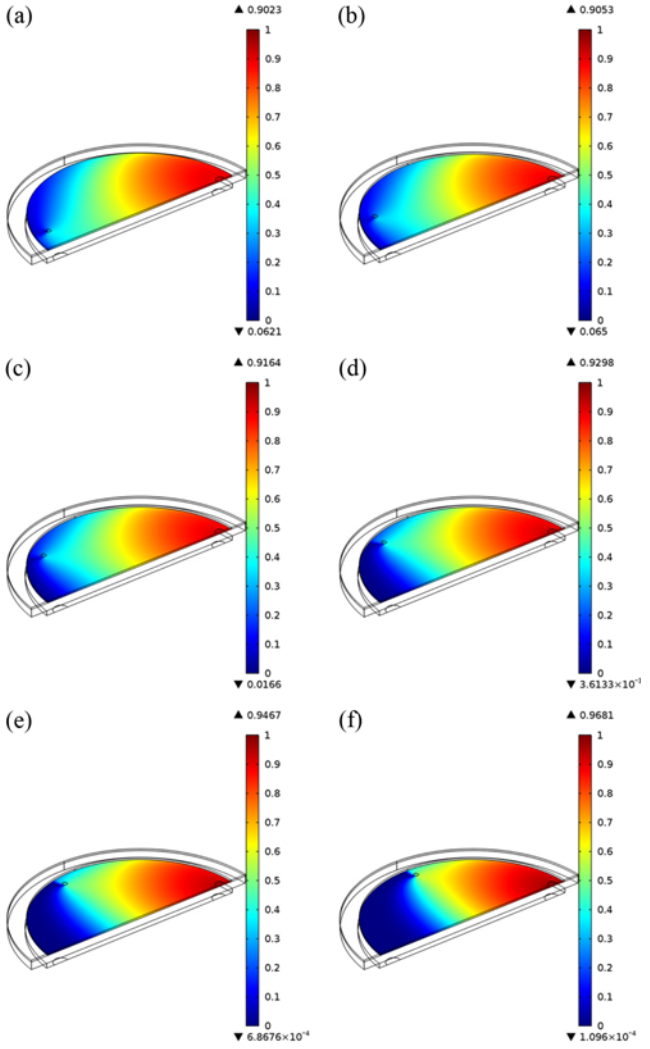

Fig. 12. Calculated values of the H_2 flux on the surface of the membrane when the number of the retentate tubes is two and θ is (a) 15°, (b) 30°, (c) 45°, (d) 60°, (e) 75°, and (f) 90°. Due to the symmetry, half of the feed tube in the center line and one retentate tube are shown in the figure.

sulting in an increase in the blue region (Diagrams d-f in Fig. 11). In addition, the increase in θ reduced the distance between the feed and the retentate tubes, as well as the residence time. Meanwhile, as shown in Fig. 12, the change of the location of the retentate tubes only slightly affected the red area around the feed tube, but a value of θ higher than 30° increased the area of the no flow zone (dark blue).

According to the above discussion, an increase in the feed tube diameter and the number of tubes enhanced the separation performance. Because the CO_2 fraction in the retentate must be higher than 90%, the fraction values were calculated for varying operating conditions and design specifications. As shown in Fig. 13, conditions employing two feed tubes, θ=45°, and a feed tube diameter of 2.45 mm guaranteed increased H_2 separation compared to the single feed tube and two retentate tube cases. The values were regressed using a second-order polynomial as a function of the total flow rate (see the caption for detailed results for the regression), and then, the flow rates for a 90% CO_2 fraction in the retentate

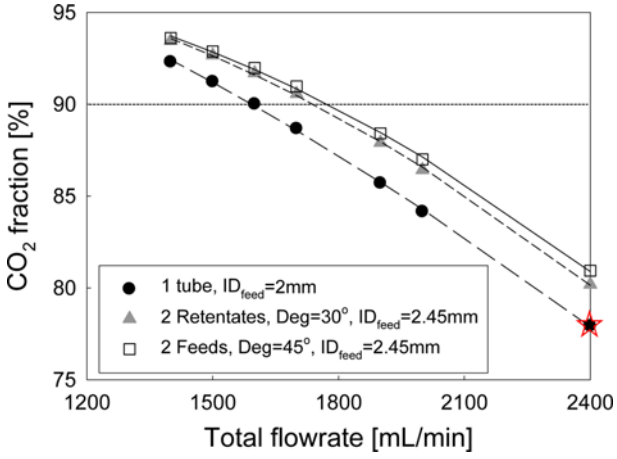

Fig. 13. CO_2 fractions in the retentate as a function of total flow rate, the number of tubes, θ, and the feed tube diameter. Regressed results for 1 tube (long dashed line), 2 retentates (short dashed line), and 2 feeds (solid line) are $y=104.7-5.4\times10^{-3}x-2.4\times10^{-6}x^2$ (R^2=0.9996), $y=97.7-3.1\times10^{-3}x-4.4\times10^{-6}x^2$ (R^2=0.9995), and $y=96.1-4.8\times10^{-3}x-4.6\times10^{-6}x^2$ (R^2=0.9992), respectively.

were calculated as 1,588.1, 1,733.9, and 1,775.5 mL/min for the single feed tube, double retentate, and double feed tube cases, respectively. Therefore, the separation performance could be increased by 11.80% [=100×(1775.5−1588.1)/1588.1].

CONCLUSIONS

CFD modeling approach was applied to predict the performance of CO_2 capture from an H_2/CO_2 binary gas mixture using a Pd-based membrane module, with respect to changes in module geometry. H_2 fluxes at the boundary between the feed chamber and the membrane were calculated by taking momentum and mass balance equations into account, while varying the flow rate, the location and the diameter of the feed tube, and the number and location of the feed and retentate tubes. Simulation results were compared to experimental data to show the effectiveness of the model, and satisfactorily demonstrated the effects of operating conditions and module structure on the performance of the module. The change of structure to the case of two feed tubes, θ=45°, and a feed tube diameter of 2.45 mm resulted in an increase in the separation performance of up to 11.80% compared to the reference conditions. In conclusion, CFD modeling can contribute to the design of an efficient CO_2 capture module by obviating an extremely large number of expensive and laborious experimental investigations.

ACKNOWLEDGEMENT

This work was supported by the "Energy Efficiency & Resources Programs" of the Korea Institute of Energy Technology Evaluation and Planning (KETEP) grant funded by the Korea government Ministry of Knowledge Economy (No. 20122010200071 for Shin D-Y and Park M-J; No. 2011201020005A for Hwang K-R and Park J-S).

NOMENCLATURE

A : surface area of membrane [m^2]
$D_{CO_2-H_2}$: binary diffusion coefficient between CO_2 and H_2 [$cm^2\ s^{-1}$]
F : volume force vector [$N\ m^{-3}$]
j_{H_2} : H_2 flux at the boundary between the feed chamber and membrane [$mol\ m^{-2}\ s^{-1}$]
l : thickness of membrane [m]
M_i : molar mass of species i [$kg\ mol^{-1}$]
$\dot{m}_{H_2}$: molar flow rate of H_2 to permeate [$mol\ s^{-1}$]
P : pressure [Pa]
ΔP : pressure difference [Pa]
Q : permeance [$mol\ m^{-2}\ s^{-1}\ Pa^{-n}$]
Q′ : permeability [$mol\ m^{-2}\ s^{-1}\ Pa^{-n}$]
R : gas constant [$J\ mol^{-1}\ K^{-1}$]
R_i : reaction rate [$kg\ m^{-3}\ s^{-1}$]
T : temperature [K]
u : linear velocity [$m\ s^{-1}$]
v : atomic diffusion volume [$cm^3\ mol^{-1}$]
x_i : composition of species i

Greek Letters

β : correlation factor
ρ : fluid density [$kg\ m^{-3}$]

Subscript

p : permeate
r : retentate
ref : reference conditions (Location 1, feed tube I.D.=2 mm, the numbers of both feed and retentate tubes=1, flow rate=2,400 mL/min, T=673 K, ΔP=2 MPa)
sf : scaling factor

REFERENCES

1. D. M. D'Alessandro, B. Smit and J. R. Long, *Angew. Chem. Int. Ed.*, **49**, 6058 (2010).
2. S.-K. Ryi, J.-S. Park, K.-R. Hwang, C.-B. Lee and S.-W. Lee, *Int. J. Hydrogen Energy*, **36**, 13769 (2011).
3. K.-R. Hwang, C.-B. Lee, S.-K. Ryi and J.-S. Park, *Int. J. Hydrogen Energy*, **37**, 6626 (2012).
4. K.-R. Hwang, S.-W. Lee, S.-K. Ryi, D.-K. Kim, T.-H. Kim and J.-S. Park, *Fuel Process. Technol.*, **106**, 133 (2013).
5. T. A. Peters, T. Kaleta, M. Stange and R. Bredesen, *J. Membr. Sci.*, **383**, 124 (2011).
6. C. V. Miguel, A. Mendes, S. Tosti and L. M. Madeira, *Int. J. Hydrogen Energy*, **37**, 12680 (2012).
7. W.-H. Chen, W.-Z. Syu, C.-I. Hung, Y.-L. Lin and C.-C. Yang, *Int. J. Hydrogen Energy*, **38**, 1145 (2013).
8. S.-K. Ryi, J.-S. Park, S.-H. Kim, S.-H. Cho, K.-R. Hwang, D.-W. Kim and H.-G. Kim, *J. Membr. Sci.*, **297**, 217 (2007).
9. H. Takaba and S.-i. Nakao, *J. Membr. Sci.*, **249**, 83 (2005).
10. A. Caravella, G. Barbieri and E. Drioli, *Chem. Eng. Sci.*, **63**, 2149 (2008).
11. J. Choi, M.-J. Park, J. Kim, Y. Ko, S.-H. Lee and I. Baek, *Korean J. Chem. Eng.*, **30**, 1187 (2013).
12. J. Boon, H. Li, J. W. Dijkstra and J. A. Z. Pieterse, *Energy Procedia*, **4**, 699 (2011).
13. M. Coroneo, G. Montante, J. Catalano and A. Paglianti, *J. Membr. Sci.*, **343**, 34 (2009).
14. W.-H. Chen, W.-Z. Syu and C.-I. Hung, *Int. J. Hydrogen Energy*, **36**, 14734 (2011).
15. S. C. Brenner and L. R. Scott, *The mathematical theory of finite element methods*, 2nd Ed. Springer-Verlag, New York (2002).
16. M. E. Celebi, F. Celiker and H. A. Kingravi, *Pattern Recognition*, **44**, 278 (2011).
17. E. N. Fuller, P. D. Schettler and J. C. Giddings, *Ind. Eng. Chem.*, **58**, 18 (1966).
18. E. N. Fuller, K. Ensley and J. C. Giddings, *J. Phys. Chem.*, **73**, 3679 (1969).
19. W.-H. Chen and P.-C. Hsu, *Int. J. Hydrogen Energy*, **36**, 9355 (2011).
20. I. P. Mardilovich, E. Engwall and Y. H. Ma, *Desalination*, **144**, 85 (2002).
21. A. Li, W. Liang and R. Hughes, *Thin Solid Films*, **350**, 106 (1999).
22. N. Itoh and W. C. Xu, *Appl. Catal. A: Gen.*, **107**, 83 (1993).
23. Y.-M. Lin, S.-L. Liu, C.-H. Chuang and Y.-T. Chu, *Catal. Today*, **82**, 127 (2003).
24. W.-H. Chen, P.-C. Hsu and B.-J. Lin, *Int. J. Hydrogen Energy*, **35**, 5410 (2010).
25. H. Gao, J. Y. S. Lin, Y. Li and B. Zhang, *J. Membr. Sci.*, **265**, 142 (2005).
26. F. Roa, J. D. Way, R. L. McCormick and S. N. Paglieri, *Chem. Eng. J.*, **93**, 11 (2003).
27. W. Liang and R. Hughes, *Catal. Today*, **104**, 238 (2005).
28. B. K. R. Nair, J. Choi and M. P. Harold, *J. Membr. Sci.*, **288**, 67 (2007).
29. L. Wang, R. Yoshiie and S. Uemiya, *J. Membr. Sci.*, **306**, 1 (2007).
30. D. Wang, J. Tong, H. Xu and Y. Matsumura, *Catal. Today*, **93-95**, 689 (2004).
31. J. Tong, Y. Matsumura, H. Suda and K. Haraya, *Sep. Purif. Technol.*, **46**, 1 (2005).
32. R. Dittmeyer, V. Höllein and K. Daub, *J. Mol. Catal. A: Chem.*, **173**, 135 (2001).
33. M. L. Bosko, D. Yepes, S. Irusta, P. Eloy, P. Ruiz, E. A. Lombardo and L. M. Cornaglia, *J. Membr. Sci.*, **306**, 56 (2007).
34. Y.-H. Chi, P.-S. Yen, M.-S. Jeng, S.-T. Ko and T.-C. Lee, *Int. J. Hydrogen Energy*, **35**, 6303 (2010).